The COOLER Code: A Novel Analytical Approach to Calculate Subcellular Energy Deposition by Internal Electron Emitters

Author(s): Mattia Siragusa, Giorgio Baiocco, Pil M. Fredericia, Werner Friedland, Torsten Groesser, Andrea Ottolenghi and Mikael Jensen
Source: Radiation Research, 188(2):204-220.
Published By: Radiation Research Society
https://doi.org/10.1667/RR14683.1
URL: http://www.bioone.org/doi/full/10.1667/RR14683.1

RADIATION RESEARCH **188**, 204–220 (2017)
0033-7587/17 $15.00

DOI: 10.1667/RR14683.1

The COOLER Code: A Novel Analytical Approach to Calculate Subcellular Energy Deposition by Internal Electron Emitters

Mattia Siragusa,[a,1,2] Giorgio Baiocco,[b] Pil M. Fredericia,[a,2] Werner Friedland,[c] Torsten Groesser,[a] Andrea Ottolenghi[b] and Mikael Jensen[a]

[a] *Hevesy Laboratory, Center for Nuclear Technologies, Technical University of Denmark, Roskilde, Denmark;* [b] *Department of Physics, University of Pavia, Pavia, Italy; and* [c] *Institute of Radiation Protection, Helmholtz Zentrum München - German Research Center for Environmental Health, Neuherberg, Germany*

Siragusa, M., Baiocco, G., Fredericia, P. M., Friedland, W., Groesser, T., Ottolenghi, A and Jensen, M. The COOLER code: A Novel Analytical Approach to Calculate Subcellular Energy Deposition by Internal Electron Emitters. *Radiat. Res.* 188, 204–220 (2017).

COmputation Of Local Electron Release (COOLER), a software program has been designed for dosimetry assessment at the cellular/subcellular scale, with a given distribution of administered low-energy electron-emitting radionuclides in cellular compartments, which remains a critical step in risk/benefit analysis for advancements in internal radiotherapy. The software is intended to overcome the main limitations of the medical internal radiation dose (MIRD) formalism for calculations of cellular S-values (i.e., dose to a target region in the cell per decay in a given source region), namely, the use of the continuous slowing down approximation (CSDA) and the assumption of a spherical cell geometry. To this aim, we developed an analytical approach, entrusted to a MATLAB-based program, using as input simulated data for electron spatial energy deposition directly derived from full Monte Carlo track structure calculations with PARTRAC. Results from PARTRAC calculations on electron range, stopping power and residual energy versus traveled distance curves are presented and, when useful for implementation in COOLER, analytical fit functions are given. Example configurations for cells in different culture conditions (V79 cells in suspension or adherent culture) with realistic geometrical parameters are implemented for use in the tool. Finally, cellular S-value predictions by the newly developed code are presented for different cellular geometries and activity distributions (uniform activity in the nucleus, in the entire cell or on the cell surface), validated against full Monte Carlo calculations with PARTRAC, and compared to MIRD standards, as well as results based on different track structure calculations (Geant4-DNA). The largest discrepancies between COOLER and MIRD predictions were generally found for electrons between 25 and 30 keV, where the magnitude of disagreement in S-values can vary from 50 to 100%, depending on the activity distribution. In calculations for activity distribution on the cell surface, MIRD predictions appeared to fail the most. The proposed method is suitable for Auger-cascade electrons, but can be extended to any energy of interest and to beta spectra; as an example, the ^{3}H case is also discussed. COOLER is intended to be accessible to everyone (preclinical and clinical researchers included), and may provide important information for the selection of radionuclides, the interpretation of radiobiological or preclinical results, and the general establishment of doses in any scenario, e.g., with cultured cells in the laboratory or with therapeutic or diagnostic applications. The software will be made available for download from the DTU-Nutech website: http://www.nutech.dtu.dk/.

INTRODUCTION

Absorbed dose is usually regarded as the primary measurement for assessment and prediction of radiation-induced biological effects. The goal of any radiation therapy is to deliver a high and lethal dose to malignant cells, while sparing normal cells. The need for accurate and precise dose planning and dosimetry is universally accepted in external radiotherapy. There is general agreement that internal radiotherapy should aim at delivering predictable and defined radiation doses to tumor targets, and that reliable estimates of the collateral radiation dose to nontargeted organs and tissues be made available. In the framework of the International Commission on Radiological Protection (ICRP) and through the work of the Medical Internal Radiation Dose (MIRD) Committee, this is now possible with acceptable precision using organ S-values, which are defined as the dose to a target region per decay in a source region (*1*), based on the reference man assumptions and using measured or extrapolated organ time-activity curves.

Adoption of the MIRD formalism becomes critical if the isotopes in question are selected to give highly localized doses, with typical particle ranges equal to or less than one

[1] Address for correspondence: Technical University of Denmark (DTU), Hevesy Laboratory, Center for Nuclear Technologies (Nutech), Risø Campus, Frederiksborgvej 399, Roskilde, Roskilde 4000 Denmark; email: masir@dtu.dk.

[2] Scholar-in-training, Radiation Research Society.

cell diameter. Here, the intracellular activity distribution becomes important, as well as a subcellular definition of source and target regions. This is taken into account in the definition of cellular S-values, that have been established by the MIRD Committee (*1*). However, the method proposed for the calculations of cellular S-values by MIRD has two main limitations: the use of the continuous slowing down approximation (CSDA) and the assumption of a spherical cell geometry. Both limitations can be overcome by the direct use of Monte Carlo codes for S-value calculations. In particular, track structure codes offer the highest possible level of details in the description of spatial energy loss in cell compartments, and any realistic geometry for such compartments can in principle be implemented.

Different research directions can be identified, which could herald advancements in the successful applications of internal radiotherapy with significant short-range particle emissions, among which are:

1. The measurement and modeling of source distributions in nonuniform targets inside the body, depending on the accumulation of radionuclide carriers in different cells (e.g., tumor vs. healthy) and cell compartments.
2. The provision of robust and generally applicable tools for dosimetry calculations at the subcellular level (cellular S-values).
3. Additional theoretical and computational tools to modify the basic concept of absorbed dose, when low-energy, cascading electron emitters are bound to critical targets such as the DNA.

Within this context, the main goal of this work was to progress in one of these directions, namely, providing a software tool to calculate subcellular doses given the distribution of radionuclides in cellular compartments, which remains a critical step in risk/benefit analysis for advancements in internal radiotherapy. The approach we propose overcomes the main limitations of the MIRD formalism, by adopting input on spatial energy loss directly derived from full Monte Carlo track structure calculations, and allowing calculations for a variety of cell geometries. The tool is intended to be accessible to everyone (preclinical and clinical researchers included), and can provide important information for the selection of radionuclides, for the interpretation of radiobiological or preclinical results, and for the general establishment of doses in any scenario, with cultured cells in laboratory or with therapeutic or diagnostic applications.

In the following, the original MIRD formalism for cellular S-values is described first. The new approach adopted in this work is then introduced, and details on each of the necessary calculation steps and ingredients (as cellular geometry or activity distribution definitions) are given in the Materials and Methods section. Simulation results (as range, stopping power, residual energy vs. traveled distance curve) obtained from electron track structure calculations with PARTRAC (PARticle TRACks) (*2*) are then presented and, when useful for implementation in the analytical approach, fit functions are given. Finally, cellular S-value predictions with the new approach are presented for different cellular geometries and activity distributions, validated against full Monte Carlo calculations with PARTRAC, and compared to MIRD standards and predictions based on different track structure calculations. In addition to calculations with monoenergetic electrons, the $_3$H case is also discussed.

The Original MIRD Formalism of Cellular S-Values

The original cellular MIRD formalism relies on the assumption of a uniform activity distribution, with radionuclide sources spread in one or more cellular compartments such as the cell nucleus, the cytoplasm or the entire cell (*1, 3, 4*). However, radiolabeled molecules able to selectively target tumor cells mostly lead to nonuniform activity distributions (*5–9*). A way to counterbalance the effects of tumor cell heterogeneity and poor penetration capabilities of radionuclide carriers was found in the use of penetrating beta emitters (*10, 11*). Nonetheless, energy deposition of long-range beta electrons affects healthy cells located in the proximity of the target. Primary Auger-electron emitters are often indicated as better candidates in highly targeted radionuclide therapies (*12–15*). Auger electrons are typical products of the results of radionuclides that decay by electron capture or have substantial internal conversion (*16*). Auger events originating from inner-shell vacancies lead to a cascade of successive transitions with several low-energy and short-range electrons (*17*), here all conveniently called Auger electrons.

The starting point to derive MIRD formalism for monoenergetic electrons consists in expressing the absorbed dose D (Gy) as:

$$D = \frac{w\tilde{A}\sum_i n_i E_i \phi_i}{m}, \quad (1)$$

where D is the absorbed dose and $\tilde{A}$ is the cumulated activity (Bq $\times$ s), n_i is the number of particles with energy E_i (keV) emitted per nuclear transition, ϕ_i is the absorbed fraction, i.e., the fraction of energy emitted from the source region that is absorbed in the target region for the ith radiation component, m is the mass of the target region (kg) and w is a constant to express D in Gy.

The MIRD formalism of organ S-values generally involves the conversion of administered activity into specific organ radiation dose. S-values are defined through the following expression, giving the absorbed dose in the target region D_{rk}:

$$D_{r_k} = \sum_h \tilde{A}_h S(r_k \leftarrow r_h), \quad (2)$$

where r_k and $r_{h\sim}$are the target and the source region, respectively, and A_h is the cumulated activity in the source region. This can be easily generalized to the cellular level, with cellular subcompartments as targets and source regions. S-values can be calculated for a fixed combination of source

and target regions replacing D in Eq. (2) with its expression given in Eq. (1), so that:

$$S(r_k \leftarrow r_h) = \frac{w \sum_i n_i E_i \phi_{i(r_k \leftarrow r_h)}}{m_{r_k}}. \quad (3)$$

To find individual terms in Eq. (3), MIRD calculates geometric reduction factors (GRFs), which provide irradiation efficacy at a certain distance from the source point in terms of the fraction of the sphere centered on the emission point that overlaps with the target volume (*1*). The absorbed fraction ϕ_i is then written as the following convolution integral:

$$\Phi_{i(r_k \leftarrow r_h)} = \frac{1}{E_i} \int_0^\infty \psi_{r_k \leftarrow r_h}(x) \cdot \left. \frac{dE}{dX} \right|_{X(E_i) - x} dx, \quad (4)$$

where $\psi_{r_k \leftarrow r_h}(x)$ is the GRF and $\left. \frac{dE}{dX} \right|_{X(E_i) - x}$ is the stopping power evaluated at $X(E_i) - x$, i.e., the residual range of a particle with initial energy E_i after a distance [linear distance (*18*)] x through the media. For electrons with energies ranging from 20 eV to 20 MeV, MIRD adopts Cole's formulas [minor changes introduced by Howell *et al.* (*19*) are not discussed here]:

$$\begin{cases} E(X) = 5.9(X + 0.007)^{0.565} + 0.00413X^{1.33} - 0.367 \\ \frac{dE}{dX}(E) = 3.316(X + 0.007)^{-0.435} + 0.0055X^{0.33} \end{cases}, \quad (5)$$

where X is the particle range, defined as the thickness of an absorber stopping 95% of incident particles (i.e., at a 5% transmission level). The units in Eq. (5) are: E in keV, X in 100 μg/cm^2 (or μm at unit density) and dE/dX in keV $\times$ cm^2/100 μg (equivalent to keV/μm at unit density). Cole's energy-loss formula has the units of a stopping power, obtained as the derivative of the energy versus range dependence measured in electron transmission experiments in air and plastic foils (*20*). In this sense it could be referred to as an ''effective'' stopping power (*18*). Aside from the adoption of Cole's formula, the convolution integral method adopted by MIRD has some well-known limitations. As the calculation of GRFs is not trivial, cellular S-values can be defined only for simple geometries. In addition to that, the adoption of the CSDA, which is implicit in Eq. (4), neglects by construction the finite range of delta rays as well as angular deflections and straggling effects, which are relevant at the subcellular level (*3, 21*). The CSDA approach might be called into question, since the energy straggling, angular deflections and delta rays cannot be neglected at the subcellular scale (*18, 22*).

For practical use, the MIRD formalism is currently implemented in the MIRDcell software (*23*), used in this work to obtain reference S-value calculations to be compared to results of the newly proposed approach. The MIRDcell tool is further described in the Materials and Methods section.

A New Analytical Approach to Calculate Cellular S-Values

The analytical method proposed in this work circumvents the limitations that arise from the use of GRFs to calculate cellular S-values. Instead, in the calculations, quantities containing information on the spatial distribution of electron emitters are used, namely the sites of radioactive decay where the primary electron track originates. Moreover, the proposed method replaces the use of Cole's effective stopping power by the adoption of energy deposition data tables derived from full Monte Carlo simulations of electron track structure with the biophysical code PARTRAC (the use of any convenient analytical expressions of energy deposition versus distance is also possible). In the proposed approach, energy-dependent terms are completely separated from the geometrical terms. The method relies on the convolution of two main terms: one related to the position of electron sources in different cellular compartments, the other to the density of deposited energy in water as a function of distance from the source. Electron energies chosen were between 0 and 50 keV. The proposed method can be naturally extended to any energy of interest, with the possibility of being optimized for Auger-emitter radiotherapy. Starting from first principles, our tool surpasses most of the problems that accompany the original MIRD method. It is based on an analytical approach, and presented results are validated with full track structure Monte Carlo calculations with the PARTRAC code. Calculations relying on this new method are entirely entrusted to COmputation Of Local Electron Release (COOLER) software, the dedicated MATLAB-based (*24*) program code. Description of the code and its validation are discussed in detail in this article Electron ranges and energy deposition data as a function of distance from the source are also obtained and discussed. Results for electron S-values as a function of energy are presented for different activity distribution scenarios and compared to MIRD predictions. The method can be generalized for continuous spectra, for example the tritium spectrum.

MATERIALS AND METHODS

The PARTRAC Code

Monte Carlo track-structure codes that simulate the electron slowing down process in an event-by-event manner can accurately describe the discrete nature of physical interactions, overcoming most of the deficiencies of the MIRD approach (*25*). Because detailed simulation of electron tracks can be time consuming, condensed history transport codes have often been employed to approach various cellular dosimetric problems (*26–32*). Among the shortcomings of using condensed history codes, we point out the adoption of large energy cutoff for electron transport, typically between 1 and 10 keV, which results in a spatial resolution of the order of the biological target.

In this work, electron track structure calculations for monoenergetic electrons emitted from point sources were performed using the event-by-event Monte Carlo code PARTRAC (*2*). PARTRAC quantitatively follows elementary processes that occur during the passage of ionizing radiation through the target. Currently, PARTRAC can simulate photons, electrons, protons, alpha particles and ion tracks in liquid water. For our purposes, it can be employed for electrons from 10 eV to 10 MeV (*2, 33*). Therefore, it appears as a natural choice for examining low-energy electrons. Interaction cross sections in liquid

water for excitation levels and ionization shells are obtained within the plane-wave Born approximation theory with a model for the dielectric function of liquid water. For energies above 10 keV, the relativistic Bethe approximation is used, while a semi-empirical correction factor handles non-Born effects for electrons below 500 eV (*34–36*). Electrons with energies below 10 eV are no longer traced and the residual energy is deposited locally.

In the experimental setup adopted by Cole to derive the effective stopping power expression adopted in the MIRD formalism for cellular S-Values, electrons in the beam are fired along a chosen single direction. *Per contra*, internal electron sources can be thought of as isotropic emitters. The two configurations can be simulated in PARTRAC; examples are shown in Fig. 1. In this work PARTRAC was used for two purposes:

1. Energy deposition-simulated data for monoenergetic electrons were obtained and successively implemented for use in COOLER. To this aim, PARTRAC was used to generate 10,000 electron tracks emitted isotropically from a point source with energies from 0 to 50 keV. Electron interactions were simulated in an 8×10^6 μm^3 water cube. To avoid the influence of statistical outliers of observed electron ranges, we dismissed from the simulations the 100 tracks depositing energy at the greatest distance from the point source (therefore, 99% of the tracks were considered). In this sense, the electron range is defined as the radial distance between the point source and the farthest interaction, after removing the 1% longest tracks. Electron range calculations obtained with this procedure are included in the results presented in this work. An analytical fit to electron energy deposition as a function of radial distance was also derived from PARTRAC data, and the decrease of electron residual energy along such distance is also shown.
2. Calculations of average energy deposition in the cellular nucleus per decay, i.e., after the emission of a single electron, for different uniform activity distributions (in the nucleus, in the entire cell or on the cell surface) were performed, by implementing selected cell geometries in PARTRAC as detailed below. Such calculations were used to check the correct implementation of PARTRAC energy deposition-simulated data in COOLER and, more generally, to validate COOLER results.

The COOLER Code

COOLER is written as a suite of MATLAB-based functions (*24*) to calculate local energy deposition, dose and S-values at the subcellular level for electrons in liquid water with energies from 0 to 50 keV.

The theoretical approach adopted relies on the following convolution:

$$E_{dep}(\rho) = \left(\tilde{A}_N * k_{density}\right)(\rho) = \int^{\tilde{A}_N}(\rho') \cdot k_{density}\left(\rho - \rho'\right)dV', \quad (6)$$

where E_{dep} is the energy deposited within the target volume (expressed in keV/decay), $\tilde{A}_N$ is the cumulated activity normalized to the total number of decays (1 decay in total), and $k_{density}$ is a function representing the density of deposited energy at the radial coordinate ρ' from the electron-emitting source. Such a method can be extended to any energy of interest and, in principle, to all charged particles and all cellular geometries.

In the three-dimensional (3D) discrete form used for the software implementation, $\tilde{A}_N$ and $k_{density}$ are given by two 3D matrices: the activity matrix describes the spatial distribution of the sites of decay in the source region, while the density matrix defines a density of deposited energy in liquid water (keV/μm^3). This second matrix originates from the interrelationship between deposited energy and distance, which reflects the concept of stopping power. Such an interrelationship is obtained through calculations with the PARTRAC track structure code (*2, 36*). Calculations associated with Eq. (6) are entrusted to MATLAB-based scripts.

COOLER allows for calculating the amount of energy delivered from well-defined source regions to various target regions, for instance, the cell nucleus or the entire cell. Currently, in terms of source and target regions, COOLER can handle cubes, spheres, ellipsoids and quasi-ellipsoids (ellipsoids lying on a flat surface, with a portion of their volume cut away, to mimic adherent cell culture conditions as detailed in the following). S-values are calculated converting E_{dep} from keV/decay to Gy/decay using information on the volume and density of the target region, which is typically the nucleus.

The COOLER code will be made available for download from DTU-Nutech website: http://www.nutech.dtu.dk/.

Activity Matrix

An entire module of COOLER is devoted to handling the distribution of the decay sites in the source region (activity matrix). Currently, this module can handle point, cubical, spherical, ellipsoidal and quasi-ellipsoidal regions, in which electron emitters are uniformly distributed. Among possible geometries for the source region, of major interest are those matching the shapes of possible cellular compartments (e.g., the cell surface, the nuclear or the entire cellular volume, see later for cellular geometry definitions). Since S-values are expressed in Gy per decay (or, equivalently, Gy Bq^{-1} s^{-1}), the total energy contained in the source region is normalized to the energy of a single electron, i.e., to one single decay. Multiplying the S-value by the total number of radioactive decays occurring within the exposure time, we obtain the total dose in Gy imparted to the selected target.

Electron Deposition Data and Density Matrix

Data on spatial energy deposition by electrons obtained from PARTRAC simulations are implemented for use in COOLER for the calculation of density matrices.

To obtain energy density functions, PARTRAC results are reprocessed, and we then score the amount of energy delivered within consecutive spherical shells, concentric with the point source. The amount of energy deposited in each shell is then divided by 10,000, giving the average result for a single electron track, and then normalized to the volume of each shell, thus obtaining the density function $k_{density}$, which is the density of deposited energy, per track, as a function of the radial distance from the electron emitter. The number of shells is fixed to 300, regardless of the initial electron energy. For electrons between 0 and 50 keV, this value provides accurate density functions in reasonable computing times. Indeed, the accuracy decreases with increasing energy: the higher the energy, the longer the range and the distance between two consecutive sites of scoring (e.g., approximately 3 nm at 5 keV and 130 nm at 50 keV).

The density matrix is then built, turning $k_{density}$ into a 3D matrix. A collection of density functions was compiled and included in COOLER for electrons with energies ranging from 0 to 50 keV.

The convolution process relies on the rescaling of physical dimensions into their corresponding virtual lengths, expressed in number of cubical voxels. This feature allows for work at different precision levels, where less precision translates into shorter computation times. The scoring of the energy deposition is performed on the basis of the geometry of the source and the target regions. S-values are calculated multiplying energy deposited in the target region in keV by the conversion factor 1.602×10^{-16} (J/keV) and dividing by the volume of the target region in μm^3 (typically the nucleus) times the density of water in kg/μm^3.

Cellular Geometries

Cellular geometries are built in COOLER through operations of selection and filling of cubical voxels of 3D null matrices. For example, a spherical cell can be identified by assigning a value of 1 to the voxels that are found within a radial distance from the center of the matrix that is equal to or less than the cell radius. Addition and

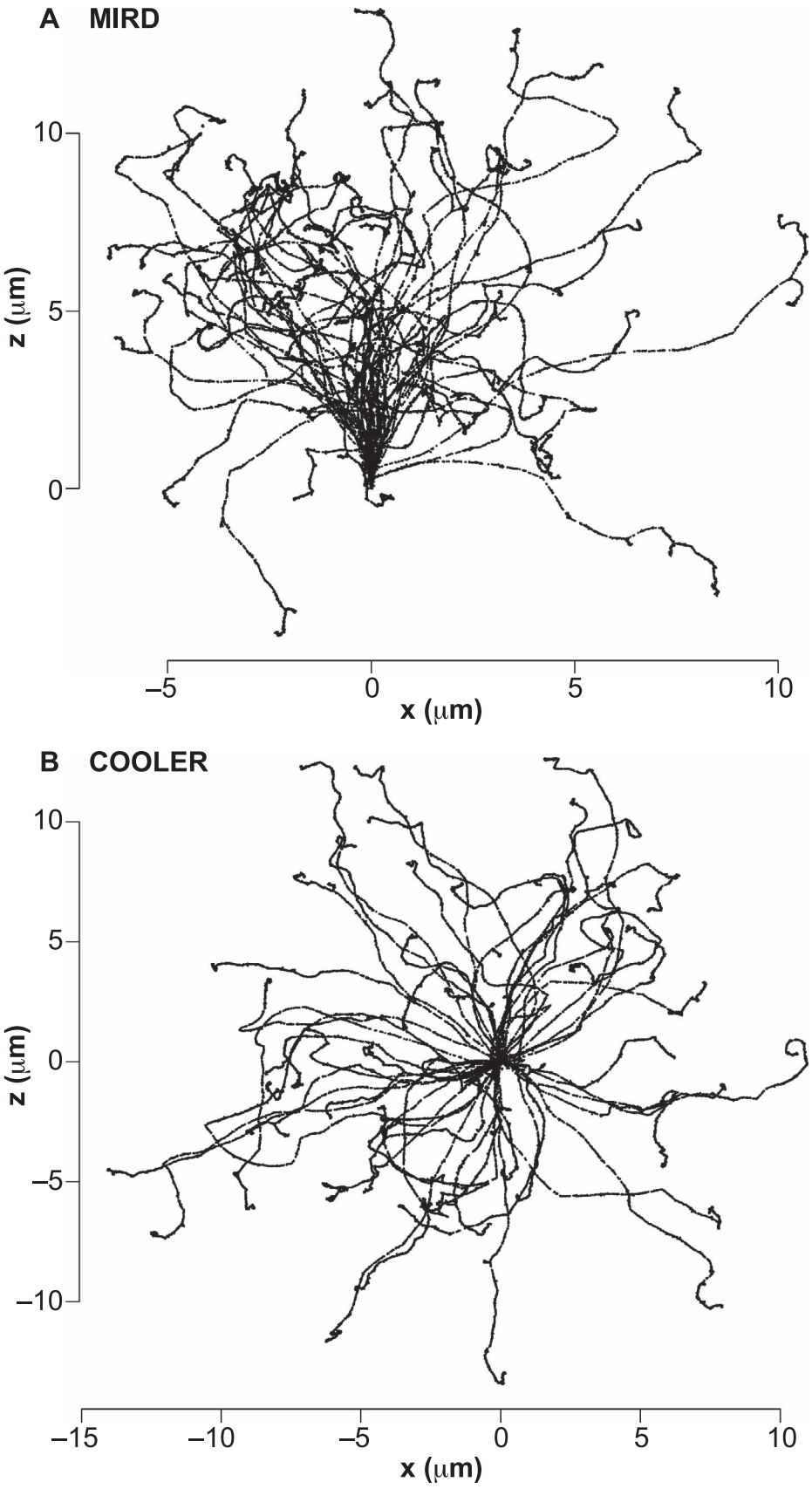

FIG. 1. 30 keV electron tracks generated in liquid water using the Monte Carlo code PARTRAC. Panel A: Experimental setup adopted by Cole (*20*) and MIRD (*1*). Panel B: The particle emission mode used in this work to determine the deposited energy against distance interrelations.

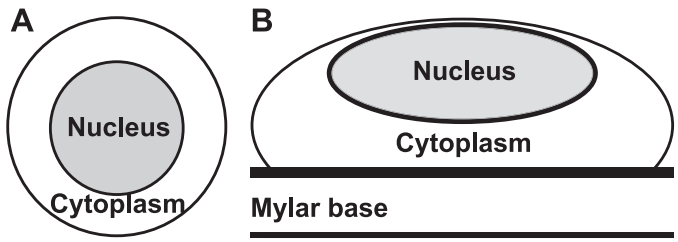

FIG. 2. Schematic representations of the cellular geometries included in COOLER. V79 cells in suspension (panel A) have a nuclear radius of 5.2 μm and a cellular radius of 7.1 μm. V79 adherent cells are shown in panel B. The thickness of the nucleus is 6.6 μm and the thickness of cytoplasm between the Mylar base and the cell nucleus is 1.4 μm. The amount of cytoplasm above the nucleus is fixed at 175 nm. The projection of the nuclear area on the Mylar base is 134 μm^2, while the nuclear and cellular volumes are assumed to be the same between panels A and B, namely 1,500 μm^3.

subtraction of voxel contents is used for more complicated geometries later introduced in this section, as cells in adherent culture. While COOLER is being developed to allow calculations with user-defined geometrical parameters, choosing among several available options, its current version includes as examples two cell models, ideally representing V79 fibroblasts under different cell culture conditions. V79 cells have been chosen for their common adoption as a radiobiological model, and the availability of information on cell geometries in different culture conditions. We adopted a spherical geometry for free-floating (suspended in culture media) V79 cells, modeling the single cell and its nucleus as concentric spheres of unit density (Fig. 2A). The cellular and nuclear radii were assumed to be 7.1 μm and 5.2 μm, respectively. However, since cells are often grown as monolayers on plastic surfaces (e.g., Mylar), we also implemented the configuration of Fig. 2B, in which the nucleus shows an ellipsoidal shape and the cell is modeled as a quasi-ellipsoid, with the cytoplasm being deformed by attachment to the Mylar layer. In this second configuration, the cell and its nucleus appear as concentric disks when seen from above. According to experimental observations (*37–40*), geometrical characteristics for the attached cells were assumed to be as follows: the nuclear thickness, the cytoplasm thickness below the nucleus (between the Mylar layer and the nucleus) and the projection of the nuclear area on the Mylar layer were set as 6.6 μm, 1.4 μm and 134 μm^2, respectively. The thickness of the cytoplasm above the nucleus was set to 175 nm. The dependence of energy deposition results on the exact positioning of the nucleus inside the cell under the adherent cell culture condition was also investigated, as detailed later. Cellular and nuclear volumes were assumed to stay constant in the two configurations, with a cell volume approximately equal to 1,500 μm^3. All values are affected by small fluctuations (generally less than 7%), depending on the geometry and the precision level set by the user when the cell model geometry is built.

Source Definition: the ^3H Case

In addition to monoenergetic electrons, COOLER can be run for sources with their own decay spectrum, thus, for example, simulating the realistic case of a cellular contamination with a beta-emitting radionuclide. Tritium data for the beta decay spectrum were taken from the freely available software Radiological Toolbox version 3.0.0 (*41*), which contains nuclear decay data assembled in ICRP Publication No. 107 (*42*). Along with spectral information, the toolbox reports a mean energy value of 5.68 keV and an end point energy of 18.59 keV.

Tritium (^3H), which is radioactive, is found in nature, but can also be produced by man-made processes (*43*). As it decays, it emits a β^- particles with a range that is usually less than the typical diameter of a cell (*44*). In this work, we computed a comparison between the use of tritium beta-decay spectrum and its mean energy only to calculate S-values in the case where the radioactivity is uniformly distributed into the entire cell, while the target region exists in the cellular nucleus. For instance, this might be the case of cells exposed to tritiated water, which is a radioactive form of water, where ^1H atoms are replaced with ^3H. Since tritiated water behavior is similar to water, it can freely diffuse in all cellular compartments, satisfying the condition of uniformity.

REFERENCE DATA

The MIRDcell V2.0.15 Tool

In collaboration with the MIRD Committee, Rutgers University (New Brunswick, NJ) developed the Java applet called MIRDcell (current version is 2.0.15), which can be accessed from http://mirdcell.njms.rutgers.edu/. The main intent of the software is to provide a user-friendly interface to calculate, for different activity distributions, the S-values and the fractions of cells that survive exposure to ionizing radiation on the basis of the calculated absorbed doses to the individual cells (*23*). In the current work, MIRDcell was employed to obtain S-values in the cellular nucleus for different uniform activity distributions. MIRDcell calculations were used to compare COOLER results with predictions consistent with the MIRD standard. The notation adopted in the software is consistent with that of this article and with MIRD Pamphlet No. 21 (*45*). In MIRDcell, monoenergetic electrons with 100% probability of emission were selected to deliver radiation to single cells. MIRDcell was run with a cellular geometry similar to that implemented for V79 floating cells, i.e., the cell and its nucleus were modeled as two concentric spheres with radii of 7 and 5 μm, respectively (the choice of the numerical values was limited by the applet running only with integer numbers). As in COOLER, cells were assumed to be composed of liquid water of unit density. The radioactivity was assumed to be uniformly distributed in the source region, selected among the cell nucleus (*N*) and the cytoplasm (*Cy*). The target region for absorbed dose calculations was the cell nucleus. As in the MIRD monograph (*1*), the effective stopping-power relationship of Cole was used for electrons. Since MIRDcell does not

directly include the $N \leftarrow Cell$ case, this was calculated by means of the volumes V_N and V_{Cy} of the different cellular compartments, as in the following equation:

$$S_{N \leftarrow Cell} = \frac{S_{N \leftarrow N} V_N + S_{N \leftarrow Cy} V_{Cy}}{V_{Cell}}. \quad (7)$$

The NIST-ESTAR Database

The NIST-ESTAR database (*46*) provides stopping power and range values for electrons in different materials, including liquid water. Data are expressed as a function of energy and given for electrons between 10 keV and 1 GeV. Collision stopping powers are estimated based on Bethe's theory (*47, 48*) and density effect corrections are calculated based on the explanation provided by Sternheimer *et. al.* (*49, 50*).

In this work, ESTAR was used to obtain electron ranges for energies between 10 and 50 keV, to be compared with PARTRAC and MIRD electron range calculations. Uncertainties of the calculated collision stopping powers are estimated to be less than 3% in water. ESTAR radiative stopping power was not considered in this work.

RESULTS

In this section, we present results for the following:

1. PARTRAC predictions for the range of monoenergetic electrons and an analytical function to fit simulated range values as a function of energy. Range values are obtained reprocessing the output of PARTRAC calculations. The fit function is implemented for use in COOLER. PARTRAC range data are compared to MIRD and NIST-ESTAR predictions;
2. The implementation in COOLER of an analytical fit function to simulated electron energy deposition data as a function of distance, and validation of the results obtained using the function instead of the simulated energy deposition data as input for COOLER calculations;
3. The residual energy versus traveled linear distance for electrons calculated from PARTRAC energy deposition data (thus, implemented in COOLER), and with the formalism adopted by MIRD;
4. Electron S-values as a function of energy, calculated taking the nuclear volume (N) as target region, with the following activity scenario: uniform activity in the nucleus ($N \leftarrow N$); uniform activity in the entire cell ($N \leftarrow Cell$); uniform activity on the cell surface ($N \leftarrow CS$); and for two different cellular geometries, simulating floating or adherent cells. S-values obtained with MIRDcell, COOLER and with full PARTRAC calculations are then compared;
5. A test of the implementation in COOLER of the ^{3}H decay spectrum, together with the comparison of results obtained using the average energy instead of the full spectrum;
6. A comparison of cellular S-values for electron emitters as obtained with COOLER, PARTRAC, MIRD and Geant4-DNA.

Electron Range

We calculated the electron range for energies between 5 and 50 keV, reprocessing the output of PARTRAC simulations. Results can be fitted using the following equation:

$$R = 0.048 \cdot E^{1.723}, \quad (8)$$

where R is the range in μm and E is the energy of the particle expressed in keV. Our results are compared with predictions from MIRD, which adopts Cole's formulas, and from the NIST-ESTAR database (referred from here on as NIST). Generally speaking, the electron range can be variously defined through concepts as the path length or the depth of penetration. The path length is the sum of all distances covered by an electron between two successive interactions before it loses all its energy (*51*). The maximal penetration depth is the distance between the electron starting point and the farthest interaction along a straight line. Thus, the maximal penetration depth is always shorter than the mean path length. The range in the CSDA can only be derived by taking the sum over the most probable path and assuming path length fluctuations are symmetric about the mean (*52*). For comparisons, we recall that range values are considered in MIRD as the maximal penetration depth of an electron beam fired along a single direction, once the 5% of electrons with the largest penetration depth are excluded. In COOLER, electron emission is radial and only the 1% of electrons having the largest penetration depth is excluded. Figure 3 shows MIRD's predictions along with range results obtained with PARTRAC, their fit via Eq. (8) and NIST's CSDA values.

Although MIRD results should refer to a ''restricted'' penetration depth, they closely reflect range values under the CSDA, which are larger than COOLER findings. Similar considerations have been previously reported (*11, 18*). Such discrepancy increases with increasing energy, but it is usually negligible, below 20 keV. It follows from Fig. 3 that between 5 and 50 keV, MIRD overestimates the range values up to 9.9% (equal to 3.99 μm) at 50 keV.

FIT to Energy Deposition Monte Carlo Data

COOLER offers the possibility to use analytical expressions of energy deposition versus distance instead of the Monte Carlo energy deposition data tables. This option is of clear interest, in that it allows for quick comparison of results from different available energy deposition patterns, without running dedicated Monte Carlo calculations, and also for particles other than electrons. To implement and validate this option, we fitted PARTRAC energy-deposition data, then we compared the S-values calculated for different

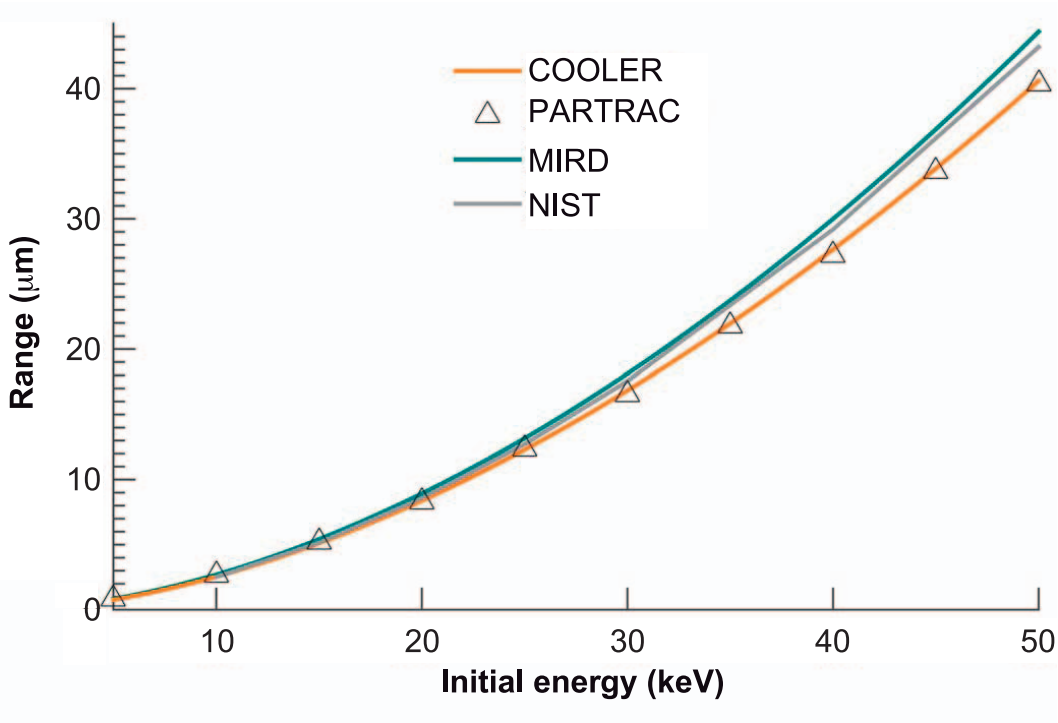

FIG. 3. Energy versus range dependence obtained by Cole (*20*), adopted by MIRD (*1*) and shown in Eq. (5) is indicated by the blue line. Such a relationship is in good agreement with NIST (*46*) range values, which are given only for energies above 10 keV (gray line). COOLER range values are shown in orange and determined by Eq. (8). Triangles represent PARTRAC simulated range values.

electron energies at fixed geometries, using as input the deposition data tables and the fitted functions. The proposed equation describing Monte Carlo data of energy deposition reads:

$$E_{dep}(\rho) = \frac{\rho_3\rho^3 + \rho_2\rho^2 + \rho_1\rho + \rho_0}{\rho^2 + q_1\rho + q_0}, \qquad (9)$$

where ρ is the radial distance from the point source given in μm. Equation (9) is plotted together with its 95% confidence bounds for electrons of 5, 25 and 50 keV in Fig. 4. The goodness of the fit was evaluated through the sum of squares due to error (SSE), the adjusted R-square (R-square) and the root mean squared error (RMSE) tests. The six parameters and statistical tests are listed in Table 2 for energies between 5 and 50 keV.

TABLE 1
Tritium Beta Spectrum, Normalized and Binned for Sampling in Monte Carlo Calculations

E_1 (keV)	E_2 (keV)	$P(E_1, E_2)$
0	1.86	0.176
1.86	3.72	0.19
3.72	5.58	0.176
5.58	7.44	0.15
7.44	9.3	0.119
9.3	11.15	0.087
11.15	13.01	0.056
13.01	14.87	0.031
14.87	16.73	0.012
16.73	18.59	0.002

Notes. Bins are uniformly distributed in energy, while the total probability of decay is normalized to one. $P(E_1, E_2)$ is the probability of emission of a beta particle with energy between E_1 and E_2.

As shown in Fig. 4, the fit nicely reproduces the data within the 95% bounds, with the exception of the initial shoulder, whose width increases with the electrons' initial energy. At 50 keV, the width of the shoulder is comparable to the cellular dimensions. This might explain the S-value discrepancies observed at the highest electron energies when Eq. (9) is compared with the PARTRAC simulated energy deposition raw data (see Table 3).

Electron Residual Energy during the Entire Stopping Process

For the test energies chosen in Fig. 4, we show in Fig. 5 how the residual electron energy decreases along the linear distance traveled from the point of origin, as it is derived from PARTRAC calculations (and therefore implemented in COOLER) and as it results with the formalism adopted by MIRD. The shape of the stopping power versus distance curves shown in Fig. 4 translates into an accelerated decrease in the residual energy when the peak in the stopping power occurs, followed by a slower decrease towards complete stopping. In the formalism adopted by MIRD the residual energy decreases faster (thus, the underlying stopping power increases) towards the end of the electron path. This comparison provides the basis for an understanding of the results in terms of S-value calculations with COOLER/PARTRAC and MIRDcell, presented below.

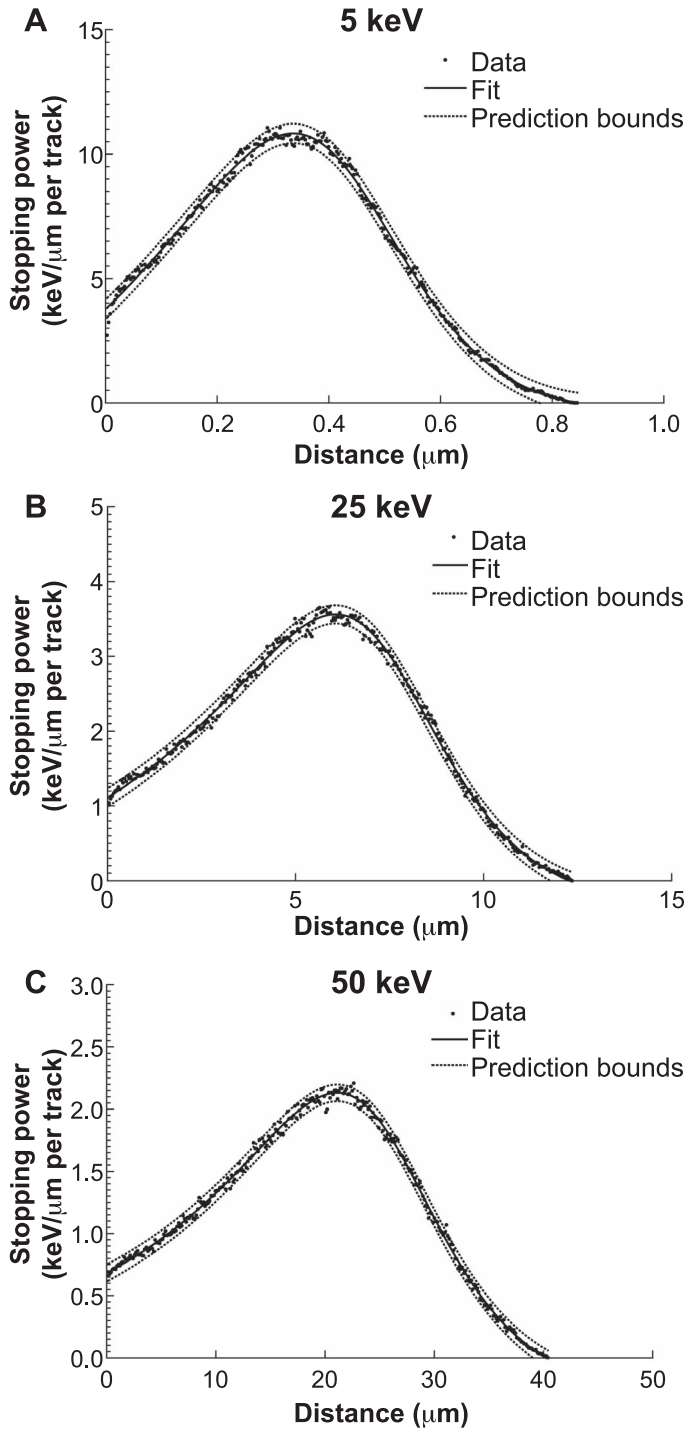

FIG. 4. Equation (9) to fit PARTRAC energy-deposition data (dots) as a function of distance is indicated by the black line, together with its 95% confidence bounds for three different initial energies, 5, 25 and 50 keV electrons (panels A–C, respectively)

S-Value Calculation

Figure 6 shows a comparison of S-values as a function of electron energy obtained through three different tools: COOLER (orange, Fig. 6A–F), PARTRAC (gray, Fig. 6A–C and E) and MIRDcell version 2.0.15 software (*23*) (blue, Fig. 6A, C and E). PARTRAC error bars are standard deviations from five independent simulation runs with a statistic of 5,000 tracks each. In Fig. 6A and B, the source region is the cell nucleus (*N*), in Fig. 6C and D the entire cell, and in Fig. 6E and F the activity is distributed only on the cell surface (*CS*). Different thicknesses of the radionuclide layer on the cell surface are used for the set of results

TABLE 2
Fit Parameters

E (keV)	p3	p2	p1	p0	q1	q0	SSE	R-square	RMSE
5	0.016	–0.026	0.007	0.003	–0.825	0.260	9.0E–05	0.997	5.6E–04
10	0.009	–0.045	0.034	0.058	–2.849	2.800	3.1E–04	0.997	1.0E–03
15	0.008	–0.077	0.120	0.341	–6.113	12.240	6.6E–04	0.997	1.5E–03
20	0.002	–0.047	0.094	1.149	–9.549	30.120	1.3E–03	0.997	2.1E–03
25	0.003	–0.069	0.217	3.094	–14.470	67.550	1.9E–03	0.997	2.5E–03
30	0.002	–0.073	0.293	7.078	–20.010	129.600	3.1E–03	0.996	3.2E–03
40	0.001	–0.101	0.707	25.640	–33.410	359.500	4.7E–03	0.997	4.0E–03
50	0.001	–0.080	0.363	71.040	–49.600	773.600	6.2E–03	0.997	4.6E–03

Notes. Equation (9) parameters are reported for different energies, spacing from 5 to 50 keV. The goodness of the model was evaluated through the sum of squares due to error (SSE), the adjusted R-square and the root mean squared error (RMSE) tests.

in Fig. 6F, while a single thin emitting surface is considered in Fig. 6E (source thickness of 0.05 μm in COOLER and PARTRAC). The target region is always the nucleus. The geometrical parameters of the two cellular configurations simulate V79 cells in suspension (Fig. 6A, C, E) or adherent culture condition (Fig. 6B, D, F). Since MIRD S-values can be computed only for spherical geometries, the comparison with MIRDcell is not possible for adherent cells, where the cell nucleus is modeled as an ellipsoid. Since the shape of the entire cell in adherent culture is modeled as a portion of ellipsoid (Fig. 2), only COOLER calculations are easily available in this case (Fig. 6D and F). When we deal with the $N \leftarrow N$ case, the cellular shape is of no interest, since the activity is contained entirely in the nucleus, and both COOLER and PARTRAC can be used for V79 adherent cells.

Based on the results shown in Fig. 6A–C and E, the convolution method implemented in COOLER is able to satisfactorily reproduce the results of full Monte Carlo calculations with PARTRAC, for all geometrical configurations and electron energies.

The role of geometry can be singled out in explaining the deviations still observed, as e.g., in Fig. 6C at 25 keV. As shown in Fig. 4 for 25 keV electrons, there is indeed a pronounced peak in the energy-deposition curve at approximately 6 μm, which is close to the radius of the V79 cell nucleus model. Concerning the higher-energy tails, the higher the electron energy the lower the accuracy of the density matrix built in COOLER. This approximation therefore plays a role in the disagreement between PARTRAC and COOLER at 40 and 50 keV in Fig. 6A and C.

Looking at Fig. 6, we can compare COOLER and PARTRAC predictions to MIRDCell results: for the sake of this comparison, we need to take into account the existence of an unavoidable source of disagreement at all energies, due to the geometrical approximations required by MIRDcell (which accepts only integer numbers for geometrical parameters of the cell). However, observed discrepancies are large only in the intermediate energy range, which suggests that differences in the shape of the energy deposition curves are to be considered as the main cause.

In general, a good agreement among all tools was expected below 10 keV for the examined cell dimensions because of the short range of low-energy electrons, which makes that only electrons originating in the nucleus contribute to the nuclear dose. A good agreement is reached for the highest electron energies, where dependence on the shape of the energy-deposition curve is weaker (if, as in our case, we neglect cross-dose effects between neighboring cells): at 50 keV the deposition peak is found at a distance of approximately 20 μm, far outside the cell itself (Fig. 4).

When different source-target configurations were compared, we observed that the $N \leftarrow Cell$ case always presents smaller S-values than $N \leftarrow N$. The reason is easily found in the increased volume of the source region for the $N \leftarrow Cell$ case. In fact, the activity normalization factor increases with the volume of the source region. When we address the

TABLE 3
S-Value Comparison between PARTRAC Raw Data and Eq. (9)

E (keV)	Floating, Eq. (9) S (Gy/decay)	Floating, PARTRAC S (Gy/decay)	Adherent, Eq. (9) S (Gy/decay)	Adherent, PARTRAC S (Gy/decay)
5	5.34E–04	5.34E–04	5.50E–04	5.51E–04
10	1.10E–03	1.10E–03	1.10E–03	1.10E–03
15	1.50E–03	1.50E–03	1.40E–03	1.40E–03
20	1.70E–03	1.70E–03	1.50E–03	1.50E–03
25	1.60E–03	1.60E–03	1.30E–03	1.30E–03
30	1.20E–03	1.20E–03	1.10E–03	1.10E–03
40	7.90E–04	8.08E–04	6.85E–04	6.98E–04
50	5.77E–04	6.10E–04	4.98E–04	5.27E–04

Notes. A comparison of S-values, obtained using Eq. (9) and PARTRAC energy deposition data, is shown for floating and adherent V79 cells. Initial energies range from 5 to 50 keV.

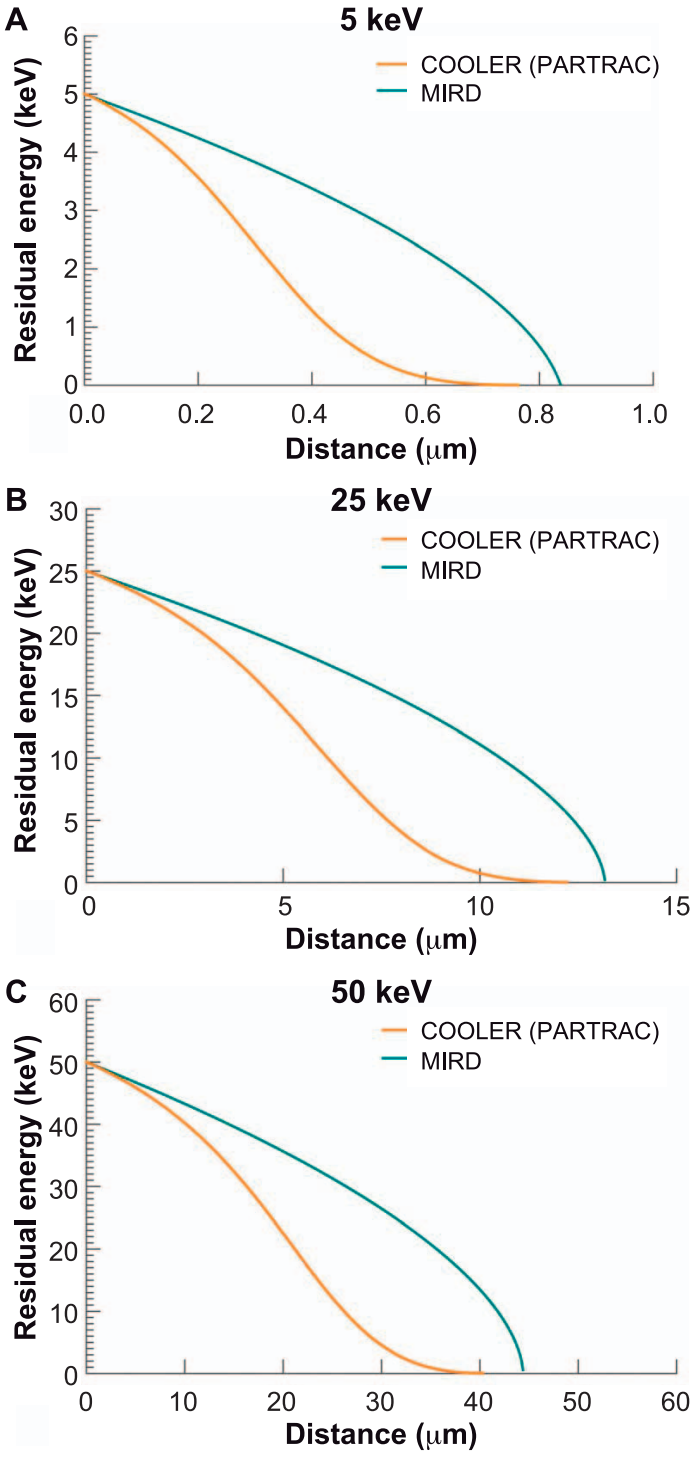

FIG. 5. Residual energy versus traveled linear distance relationships, calculated from COOLER (PARTRAC) energy deposition data tables (orange lines) and with the formalism adopted by MIRD (blue lines), are shown for 5, 25 and keV electrons (panels A–C, respectively).

N←*CS* case, a further decrease in S-values is observed, which is mainly due to the location of radionuclide sources: only electrons not getting stopped in the cytoplasm reach the target nucleus and contribute to the dose. In the suspension culture condition, when spherical symmetry is maintained, electrons with the same starting energy have the same probability to reach the nucleus, regardless of their location on the emitting surface. As a consequence, a maximum appears in the S-value relative to the initial energy relationship shown in Fig. 6E, even if at an increased energy with respect to what can be seen for the *N*←*N* or *N*←*Cell* cases. The decrease in S-values is even more

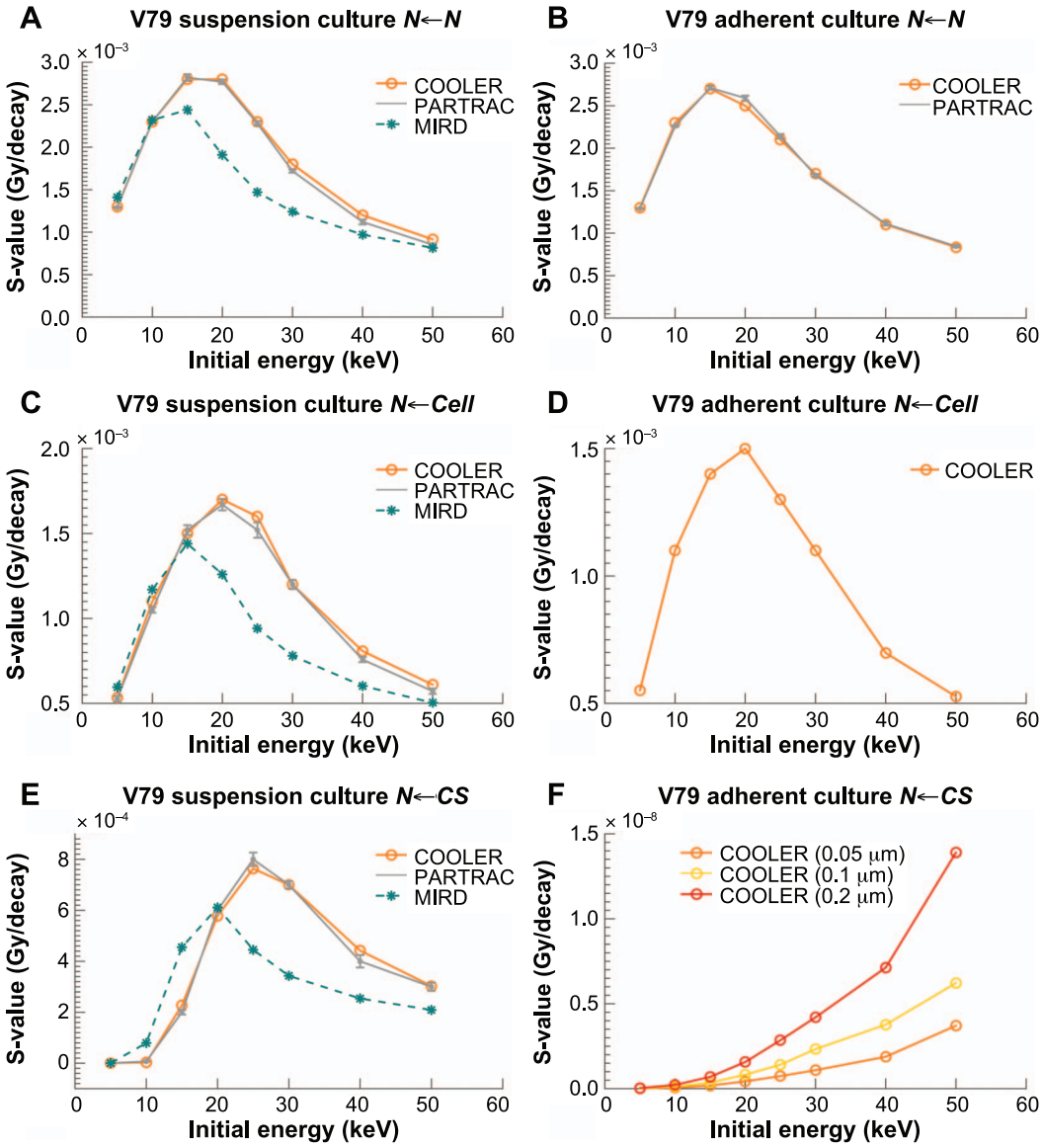

FIG. 6. Comparison of S-values as a function of electron energy obtained through three different tools: COOLER (orange, in all panels), PARTRAC (gray, panels A–C and E) and MIRDcell software (*23*) (blue, panels A, C and E). PARTRAC error bars are standard deviations from five independent simulation runs with a statistic of 5,000 tracks each. In panels A and B the source region is the cell nucleus (*N*), in panels C and D the entire cell, and in panels *E* and *F* the activity is distributed only on the cell surface (*CS*). Different thicknesses of the radionuclide layer on the cell surface are used for the set of results in panel F, while a single thin emitting surface is considered in panel E (source thickness of 0.05 μm). The target region is always the nucleus. The geometrical parameters of the two cellular configurations simulate V79 cells in suspension (panels A, C and E) or adherent culture condition (panels B, D and F). Since MIRD S-values can be computed only for spherical geometries, the comparison with MIRDcell is not possible for adherent cells, where the cell nucleus is modeled as an ellipsoid. Since the shape of the entire cell in adherent culture is modeled as a portion of ellipsoid (Fig. 2), only COOLER calculations are easily available in this case and shown in panels D and F. For the *N*←*N* case, the cellular shape is of no interest, since the activity is contained entirely in the nucleus, and both COOLER and PARTRAC can be used for adherent V79 cells.

evident for the *N*←*CS* case in the adherent culture condition (Fig. 6F), when S-values are of the order of 10^{-8} (a factor of 10^{-4} smaller than for the same activity distribution in the spherical configuration). Also, a different trend is observed: in absence of spherical symmetry, electrons with the same initial energy reach the target nucleus with very different residual energy to deposit, depending on the source location and on the electron path in the cytoplasm. No maximum is observed, but rather a constant increase of S-values up to 50 keV electron energy. In Fig. 6F we also show S-values calculated for different thicknesses of the radionuclide layer on the cell surface. If such thickness is increased, the S-

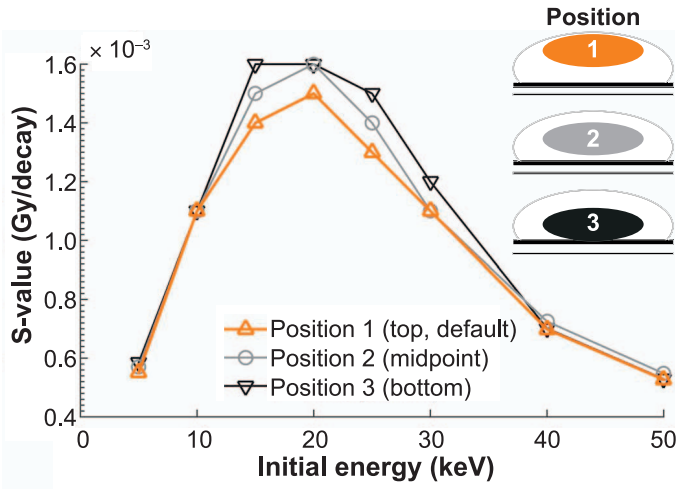

FIG. 7. Dependence of S-value calculations from cell nucleus position within V79 adherent cells is shown. Geometrical volumes are kept constant, while only the vertical position of the cell nucleus is changed. In position 1 the amount of cytoplasm beneath the cell nucleus corresponds to 1.4 μm. Position 2 indicates that the nucleus floats at an intermediate vertical position with a 0.7 μm distance between the Mylar base and the bottom of the nucleus. In position 3 the nucleus lies on the bottom of the cell.

value for a given electron energy is also increased. This is due to the fact that the increased overall activity (and therefore, the higher number of electrons which have the chance to reach the nucleus and deposit energy) prevails on the increase of the normalization constant (i.e., the number of decays) in the calculation of Gy/decay values.

Cell geometrical parameters are based on experimental measurements. In this way, we created reliable average configurations for V79 cells in different culture conditions. Figure 7 shows S-value calculations for adherent V79 cells in the *N←Cell* case for different positions of the cell nucleus. Position 1 is the default setting, with a 1.4 μm thickness of cytoplasm beneath the cell nucleus [see (*37*) and Materials and Methods]. Position 2 corresponds to a nucleus at an intermediate vertical position, with a 0.7 μm distance between the Mylar base and the bottom of the nucleus. Position 3 represents the less realistic situation, in which the nucleus lies on the bottom of the cell touching the Mylar surface. Changes in S-values are observed depending on the nuclear position in the energy range of 15–30 keV, with differences up to 15%, found to be maximal at 25 keV. For the same reasons given when we compared COOLER to MIRDCell results, no change is seen below 10 keV, which is due to the short electron range. A small and negligible S-value dependence on the positioning of the nucleus is observed at 40 and 50 keV, where the energy deposition peak is far outside the cell. This set of results is included to emphasize the importance of modeling the nuclear position correctly.

The ^{3}H Case

We computed S-values in the *N←Cell* activity scenario comparing results obtained with the use of tritium beta-decay spectrum and of its mean energy. Adopting the spherical geometry for V79 cells in suspension, we obtained the following S-values: 6.08×10^{-4} Gy/decay for the full spectrum and 6.07×10^{-4} Gy/decay using only the mean energy. The chosen modeling conditions allow us to assume totally uniform energy deposition in the media. Under these circumstances, nuclear dimensions can be disregarded, since the deposited energy increases with the nuclear size, so that the S-value remains constant. In other words, a second cell with radial dimensions equal to 3 and 7.1 μm for the nucleus and the entire cell, respectively, would still provide the same result for the S-value. These conditions hide the differences between the use of the full spectrum or just the mean energy. Experimentally, such conditions can often be reached through a uniform distribution of the activity, which is the case of tritiated water.

Comparison to S-Value Calculation with Geant4-DNA

In this section, we present the comparison among S-value results obtained with COOLER, PARTRAC, MIRD and Geant4-DNA. Results with Geant4-DNA (Fig. 8) are taken from (*53*) for the *N←N* and *N←CS* cases, with a spherical cell geometry (cell radius 5 μm; nucleus radius 4 μm). COOLER and PARTRAC results were obtained from dedicated calculations with the same cell model. Deviations from the MIRD standards were also found with Geant4-DNA, and, as previously discussed, can ultimately be traced back to the different pattern of energy deposition obtained with the MIRD formalism or with full track structure calculations. Discrepancies between COOLER/PARTRAC and Geant4-DNA were also observed, with Geant4-DNA predictions being often intermediate among COOLER/PARTRAC and MIRD results, but following the same trend. Such discrepancies can be attributed to the adoption of different cross-section datasets for electron interactions

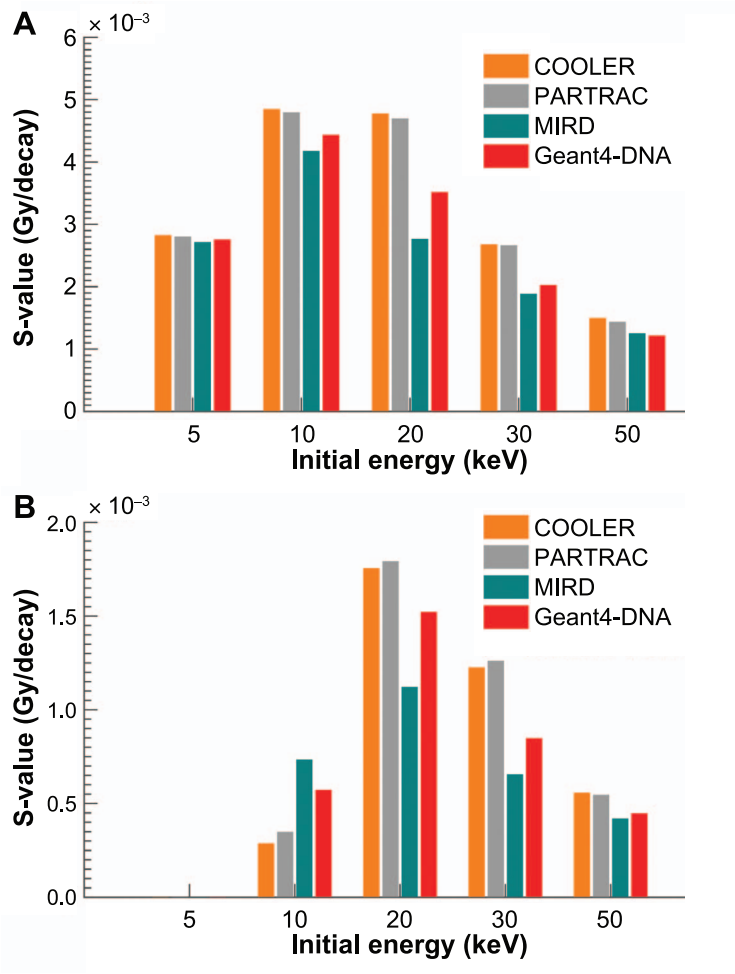

FIG. 8. A comparison of cellular S-values for electron emitters, obtained with COOLER (orange), PARTRAC (gray), MIRD (blue) and Geant4-DNA (red) is shown. Results with Geant4-DNA were obtained from (*53*) for the $N \leftarrow N$ (panel A) and $N \leftarrow CS$ (panel B) cases, with a spherical cell geometry (cell radius 5 μm; nucleus radius 4 μm). COOLER/PARTRAC results were obtained from dedicated calculations with the same cell model.

and/or of a combination of models with the need of interpolation.

CONCLUSIONS

Absorbed dose calculations in nuclear medicine are conventionally based on the formalism of the S-values introduced by the MIRD Committee. The integral method adopted for low-energy electron emitters has some well-known limitations, such as the employment of Cole's effective stopping power, the assumption of CSDA and the use of geometric reduction factors, which can be easily calculated only for simple geometries. These limitations suggest that Monte Carlo codes with low energy cutoffs for electron transport and more degrees of freedom in the geometry implementation are more suitable for S-value calculations. Among Monte Carlo programs, event-by-event codes like PARTRAC are preferred to condensed-history codes for cellular S-value calculations.

Common concerns related to Monte Carlo simulations are typically the computing time, the availability of the program and the possibility to implement new functions from scratch, such as cellular geometries or activity distributions, which is no small task. Thus, while Monte Carlo codes can provide accurate S-values, they are normally beyond the practical reach of the preclinical and clinical researcher. For these reasons, we developed the analytical tool COOLER for calculations of electron energy deposition at the subcellular level, which employs PARTRAC results as input and is validated through dedicated full Monte Carlo calculations. The adopted method can be extended to electrons (and in principle other particles) of any energy of interest and to geometries where the geometrical reduction factors do not exist or may be ill defined.

Values for the range of electrons are defined in this work as the maximal penetration depth of electrons emitted isotropically from a point source in water, once the 1% of electrons with the largest penetration depths are excluded to avoid the influence of statistical outliers. Range values were

obtained in PARTRAC and implemented in COOLER through an analytical fit function. Such values were compared to MIRD and NIST-ESTAR predictions. The range results showed discrepancies between MIRD (Cole) and COOLER (PARTRAC) increase with the energy, but were usually negligible, below 20 keV, and COOLER range values were up to 6.76% shorter than MIRD findings at 50 keV. MIRD results are always in good agreement with the NIST-ESTAR predictions. However, we are unable to perform an accurate comparison between MIRD and COOLER, since they employ different geometrical setups and different range definitions. NIST-ESTAR predictions are theoretically derived from Bethe's theory.

To promote the use of COOLER, we implemented realistic geometries for the chosen V79 cell model (a commonly adopted radiobiological model) under two different culture conditions, namely a spherical geometry for free-floating cells and a quasi-ellipsoidal configuration for cells growing as monolayers on plastic surfaces. The code will be further developed to accept user-defined geometrical parameters in a variety of possible configurations.

The approach adopted in COOLER for S-value calculations relies on the convolution of two main terms: the first is related to the distribution of electron sources in different cellular compartments; the second, which is derived from PARTRAC simulations, relates to the density of deposited energy in liquid water as a function of the radial distance from the source. This direct convolution method is validated against full PARTRAC simulations.

The largest discrepancies between COOLER and MIRD generally arise for electrons between 25 and 30 keV, where the magnitude of disagreement in S-values are of the order of 50% for $N \leftarrow N$, 70% for or $N \leftarrow Cell$, and up to 100% for the or $N \leftarrow CS$ activity scenarios. As expected, MIRD predictions seem to fail the most for calculations for activity distribution on the cell surface. Energy deposition results for electrons in this energy range present the highest dependence on the geometry, due to the shape of the deposited energy versus distance curve. For these energies deposition peaks are located between 2.5 and 6 μm; such distances are comparable to the radial dimensions of the cells. We recommend that extra attention be given when modeling the position of the target. In our simulations for V79 adherent cells, the ambiguous positioning of the cell nucleus led to discrepancy in the S-values up to 15%.

In addition to the comparison with MIRD standards, a dedicated comparison with S-value calculations with Geant4-DNA is also presented. Discrepancies between COOLER (based on PARTRAC) and Geant4-DNA predictions further highlight the dependence of S-values on the underlying electron energy deposition pattern, which in turn depends on interaction cross sections or models implemented in the track structure code. To possibly take this dependence into account in future calculations, COOLER is not pegged to PARTRAC and can work with any Monte Carlo code. An easy way to compare results between COOLER and other programs consists of selecting as input for COOLER analytical expressions for the deposited energy as a function of radial distance obtained from different Monte Carlo codes. In this work, we also provide an example of an analytical equation to fit PARTRAC energy-deposition data for electrons.

From the perspective of an experimental validation of our results, it must be reiterated that direct dosimetry at the subcellular level remains impossible to perform. Indirect benchmarks of our results versus e.g., Geant4-DNA predictions can be derived from the validation of the track structure code [in terms of implemented electron cross sections, e.g., ref. (*54*)], or from the measurement of biological outcome of cell exposure and correlation of simulated dose data to measurements of chosen radiobiological end points [e.g., DNA damage calculated with PARTRAC (*35*)]. Results such as those of this work or obtained in the future by using the COOLER code certainly pave the way for future investigations including radiobiological measurements.

COOLER was developed starting from monoenergetic electron sources, but it can also accept beta decay spectra. In this work, we have shown an example of how COOLER handles the use of continuous electron energy distribution resulting from tritium decay. In particular, the same S-value is found regardless of the use of the tritium spectrum or of its mean energy. As tritiated water freely diffuses in all cell compartments, leading to uniform activity distributions, and due to the emission of solely short range electrons, all calculations were performed under totally uniform energy deposition conditions. From such calculations, we maintain that in many experimental situations involving low energy electron emitters, information on the full decay spectrum is not needed, since uniform energy deposition conditions are granted and the use of the mean energy is often sufficient to the scope. Experimentally, such conditions can often be reached through a uniform distribution of the activity, which is the case of tritiated water.

As mentioned, extension of the code to other particles is possible, as well as to radionuclides generating mixed-field radiation or initiating a decay chain, provided that decay and spatial energy deposition data are implemented.

In this work, we have established a new analytical method to calculate energy deposition by electrons at the subcellular level, avoiding the limitations related to Cole's formula for electron stopping power and the use of geometric reduction factors. The tool we provide is demonstrated to correctly address a variety of cell geometries and activity distributions, taking as input analytical fit functions for electron range values and energy deposition data obtained from Monte Carlo calculations. COOLER provides the best possible expression of cellular S-values, limited only to the precision by which the cellular geometry can be described. In the current version of the code, we consider only uniform activity distributions in different cellular compartments (or

on the cellular surface). Calculations are limited to a single cell model, with no dose contribution to target nuclei coming from activity in neighboring cells or in the intercellular environment. Both these limitations will be overcome in future developments of the tool.

The use of COOLER is much simpler than the use of a Monte Carlo code and this makes it useful both for scientists and the medical personnel concerned with S-value calculations. A user-friendly graphical interface will be developed, and the software will be made available for download from the DTU-Nutech website: http://www.nutech.dtu.dk/.

ACKNOWLEDGMENTS

We thank the staff scientists and technicians of the Hevesy Laboratory at the Technical University of Denmark and the scientists of the Radiobiology and Radiation Biophysics group of the University of Pavia. We also thank Prof. Michael Dingfelder, Department of Physics, East Carolina University, Greenville, NC, for discussion on the issue of electron cross sections for track structure calculations.

Received: November 9, 2016; accepted: April 11, 2017; published online: June 16, 2017

REFERENCES

1. Howell RW, Dandamudi WR, Bouchet L, Bloch W, Goddu SM. MIRD cellular S values. Reston, VA: Society of Nuclear Medicine; 1997.
2. Friedland W, Dingfelder M, Kundrát P, Jacob P. Track structures, DNA targets and radiation effects in the biophysical Monte Carlo simulation code PARTRAC. Mutat Res 2011; 711:28–40.
3. Kassis AI. The MIRD approach: remembering the Limitations. J Nucl Med. 1992; 33:781–2.
4. Howell RW. The MIRD schema: from organ to cellular dimensions. J Nucl Med. 1994; 35:531–3.
5. Makrigiorgos GM, Ito S, Baranowska-Kortylewicz J, Vinter DW, Iqbal A, Van den Abbeele AD, et al. Inhomogeneous deposition of radiopharmaceuticals at the cellular level : experimental evidence and dosimetric implications. J Nucl Med 1990; 31:1358–63.
6. Makrigiorgos GM, Baranowska-Kortylewicz J, den Abbeele AD, Ito S, Vinter DW, Adelstein SJ, et al. Microscopic spatial inhomogeneity of radiopharmaceutical deposition in mammalian tissues: dosimetry at the cellular level and comparison with conventional dosimetry. Radiat Prot Dosimetry 1990; 31(1–4): 319–24.
7. Griffiths GL, Govindan S V., Sgouros G, Ong GL, Goldenberg DM, Mattes MJ. Cytotoxicity with Auger electron-emitting radionuclides delivered by antibodies. Int J Cancer 1999; 81:985–92.
8. Neti PVS V, Howell RW. Log normal distribution of cellular uptake of radioactivity: implications for biologic responses to radiopharmaceuticals. J Nucl Med 2006; 47:1049–58.
9. Kriehuber R, Riedling M, Simkó M, Weiss DG. Cytotoxicity, genotoxicity and intracellular distribution of the Auger electron emitter 65Zn in two human cell lines. Radiat Environ Biophys 2004; 43:15–22.
10. Kassis AI. Therapeutic radionuclides: biophysical and radiobiologic principles. Semin Nucl Med 2008; 38:358–66.
11. Emfietzoglou D, Bousis C, Hindorf C, Fotopoulos A, Pathak A, Kostarelos K. A Monte Carlo study of energy deposition at the sub-cellular level for application to targeted radionuclide therapy with low-energy electron emitters. Nucl Instrum Methods Phys Res B 2007; 256:547–53.
12. Kassis AI. The amazing world of Auger electrons. Int J Radiat Biol 2004; 80:789–803.
13. Fischer T, Schomacker K, Schicha H. Diethylstilbestrol (DES) labeled with Auger emitters: potential radiopharmaceutical for therapy of estrogen receptor-positive tumors and their metastases? Int J Radiat Biol 2008; 84:1112–22.
14. Yasui LS. Molecular and cellular effects of Auger emitters: 2008–2011. Int J Radiat Biol 2012; 88:864–70.
15. Kassis AI. Molecular and cellular radiobiological effects of Auger emitting radionuclides. Radiat Prot Dosimetry 2011; 143:241–7.
16. Kassis AI. Cancer therapy with Auger electrons: are we almost there? J Nucl Med 2003; 44:1479–81.
17. Bambynek W, Crasemann B, Fink RW, Freund HU, Mark H, Swift CD, et al. X-ray fluorescence yields, Auger, and Coster-Kronig transition probabilities. Rev Mod Phys 1972; 44:716–813.
18. Emfietzoglou D, Kostarelos K, Hadjidoukas P, Bousis C, Fotopoulos A, Pathak A, et al. Subcellular S-factors for low-energy electrons: a comparison of Monte Carlo simulations and continuous-slowing-down calculations. Int J Radiat Biol 2008; 84:1034–44.
19. Howell RW, Rao D V, Sastry KS. Macroscopic dosimetry for radioimmunotherapy: nonuniform activity distributions in solid tumors. Med Phys 1989; 16:66–74.
20. Cole A. Absorption of 20-eV to 50,000–eV Electron beams in air and plastic. Radiat Res 1969; 38:7–33.
21. Nikjoo H, Emfietzoglou D, Charlton DE. The Auger effect in physical and biological research. Int J Radiat Biol 2008; 84:1011–26.
22. Nikjoo H, Uehara S, Emfietzoglou D, Cucinotta FA. Track-structure codes in radiation research. Radiat Meas 2006; 41:1052–74.
23. Vaziri B, Wu H, Dhawan AP, Du P, Howell RW. MIRD pamphlet No. 25: MIRDcell V2.0 software tool for dosimetric analysis of biologic response of multicellular populations. J Nucl Med 2014; 55:1557–64.
24. MATLAB version 8.5.0.197613 (R2015a). Natick, MA: MathWorks Inc.; 2015. (http://bit.ly/2qcukNL)
25. Bousis C, Emfietzoglou D, Hadjidoukas P, Nikjoo H. A Monte Carlo study of cellular S-factors for 1 keV to 1 MeV electrons. Phys Med Biol 2009; 54:5023–38.
26. Artman T, Lundqvist H, Westlin J-E, Carlsson J. Radiation doses to the cell nucleus in single cells and cells in micrometastases in targeted therapy with 131 I labeled ligands or antibodies. Int J Radiat Oncol Biol Phys 2000; 46:1025–36.
27. Stewart RD, Wilson WE, McDonald JC, Strom DJ. Microdosimetric properties of ionizing electrons in water: a test of the PENELOPE code system. Phys Med Biol 2002; 47:79–88.
28. Coulot J, Ricard M, Aubert B. Validation of the EGS usercode DOSE3D for internal beta dose calculation at the cellular and tissue levels. Phys Med Biol 2003; 48:2591–602.
29. Syme a M, Kirkby C, Riauka T a, Fallone BG, McQuarrie S a Monte Carlo investigation of single cell beta dosimetry for intraperitoneal radionuclide therapy. Phys Med Biol 2004; 49:1959–72.
30. Hindorf C, Emfietzoglou D, Lindén O, Kostarelos K, Strand S-E. Internal microdosimetry for single cells in radioimmunotherapy of B-cell lymphoma. Cancer Biother Radiopharm 2005; 20:224–30.
31. Hindorf C, Emfietzoglou D, Lindén O, Bousis C, Fotopoulos A, Kostarelos K, et al. Single-cell dosimetry for radioimmunotherapy of B-cell lymphoma patients with special reference to leukemic spread. Cancer Biother Radiopharm 2007; 22:357–66.
32. Pacilio M, Lanconelli N, Lo Meo S, Betti M, Montani L, Torres Aroche LA, et al. Differences among Monte Carlo codes in the calculations of voxel S values for radionuclide targeted therapy and analysis of their impact on absorbed dose evaluations. Med Phys 2009; 36:1543–52.

33. Li WB, Friedland W, Pomplun E, Jacob P, Paretzke HG, Lassmann M, et al. Track structures and dose distributions from decays of (131)I and (125)I in and around water spheres simulating micrometastases of differentiated thyroid cancer. Radiat Res 2001; 156:419–29.

34. Dingfelder M, Hantke D, Inokuti M, Paretzke HG. Electron inelastic-scattering cross sections in liquid water. Radiat Phys Chem 1999; 53:1–18.

35. Dingfelder M, Ritchie RH, Turner JE, Friedland W, Paretzke HG, Hamm RN. Comparisons of calculations with PARTRAC and NOREC: transport of electrons in liquid water. Radiat Res 2008; 169:584–94.

36. Alloni D, Campa A, Friedland W, Mariotti L, Ottolenghi A. Track structure, radiation quality and initial radiobiological events: Considerations based on the PARTRAC code experience. Int J Radiat Biol 2012; 88:77–86.

37. Ottolenghi a, Monforti F, Merzagora M. A Monte Carlo calculation of cell inactivation by light ions. Int J Radiat Biol 1997; 72:505–13.

38. Townsend KM, Stretch A, Stevens DL, Goodhead DT. Thickness measurements on V79-4 cells: a comparison between laser scanning confocal microscopy and electron microscopy. Int J Radiat Biol 1990; 58:499–508.

39. Townsend KMS, Marsden SJ. Nuclear area measurement on viable cells, using confocal microscopy. Int J Radiat Biol 1992; 61:549–51.

40. Bettega D, Calzolari P, Doglia SM, Dulio B, Tallone L, Villa AM. Technical report: Cell thickness measurements by confocal fluorescence microscopy on C3H10T1/2 and V79 cells. Int J Radiat Biol 1998; 74:397–403.

41. Eckerman KF, Sjoreen AL. Radiological toolbox user's guide. Washington, D.C.: U.S. Nuclear Regulatory Commission; 2013. (http://bit.ly/2qWP7E6)

42. Eckerman KF, Endo A. ICRP Publication 107: Nuclear decay data for dosimetric calculations. Ann ICRP 2008; 38:7–96.

43. Radiation protection. Emerging issues on tritium and low energy beta emitters. Report No. 152. Proceedings of the EU Scientific Seminar; 2007; Luxembourg: European Commission; 2007. (http://bit.ly/2rAIIiJ)

44. Alloni D, Cutaia C, Mariotti L, Friedland W, Ottolenghi A. Modeling dose deposition and DNA damage due to low-energy beta(–) emitters. Radiat Res 2014; 182:322–30.

45. Bolch WE, Eckerman KF, Sgouros G, Thomas SR. MIRD pamphlet No. 21: a generalized schema for radiopharmaceutical dosimetry–standardization of nomenclature. J Nucl Med 2009; 50:477–84.

46. Berger MJ. ESTAR, PSTAR, and ASTAR: Computer programs for calculating stopping-power and range tables for electrons, protons, and helium ions. Gaithersburg, MD: National Institute of Standards and Technology; 1992.

47. Bethe H. Zur Theorie des Durchgangs schneller Korpuskularstrahlung durch Materie. Ann Phys 1930; 5:325–400.

48. Bethe H. Bremsformel für Elektronen relativistischer Geschwindigkeit. Zeitschrift für Phys 1932; 76:293–9.

49. Sternheimer RM. The density effect for the ionization loss in various materials. Phys Rev 1952; 88:851–9.

50. Sternheimer RM, Berger MJ, Seltzer SM. Density effect for the ionization loss of charged particles in various substances. At Data Nucl Data Tables 1984; 30:261–71.

51. Rogers DWO. Introduction to radiological physics and radiation dosimetry by F. H. Attix. Med Phys 1987; 14:692

52. Berger M, Seltzer S. Tables of energy-losses and ranges of electrons and positrons. NASA Report No. SP-3012. Washington, DC: National Aeronautics and Space Administration; 1964

53. Sefl M, Incerti S, Papamichael G, Emfietzoglou D. Calculation of cellular S-values using Geant4-DNA: the effect of cell geometry. Appl Radiat Isot 2015; 104:113–23.

54. Meesungnoen J, Jay-Gerin J-P, Filali-Mouhim A, Mankhetkorn S. Low-energy electron penetration range in liquid water. Radiat Res 2002; 158:657–60.